This is the accepted manuscript made available via CHORUS. The article has been published as:

Giant orbital polarization of math xmlns="http://www.w3.org/1998/Math/MathML">msup>mrow>mi>Ni/mi>/mrow>mrow>mn>2/mn>mo>+/mo>/mrow>/msup>/math> in a square planar environment

Prithwijit Mandal, Ranjan Kumar Patel, Dibyata Rout, Rajdeep Banerjee, Rabindranath Bag, Koushik Karmakar, Awadhesh Narayan, John W. Freeland, Surjeet Singh, and Srimanta Middey

Phys. Rev. B **103**, L060504 — Published 17 February 2021

DOI: 10.1103/PhysRevB.103.L060504

Giant orbital polarization of Ni^{2+} in square planar environment

Prithwijit Mandal,[1,*] Ranjan Kumar Patel,[1,*] Dibyata Rout,[2] Rajdeep Banerjee,[3] Rabindranath Bag,[2] Koushik Karmakar,[2] Awadhesh Narayan,[3] John W. Freeland,[4] Surjeet Singh,[2] and Srimanta Middey[1,†]

[1]*Department of Physics, Indian Institute of Science, Bengaluru 560012, India*
[2]*Department of Physics, Indian Institute of Science Education and Research, Pune, Maharashtra 411008, India*
[3]*Solid State and Structural Chemistry Unit, Indian Institute of Science, Bengaluru 560012, India*
[4]*Advanced Photon Source, Argonne National Laboratory, Argonne, Illinois 60439, USA*

Finding large orbital polarization in Ni based oxides has become a topic of paramount interest in recent years due to the prospect of finding superconductivity. In this work, we investigate electronic structure of single-crystalline samples of Sr_2CuO_3 and Ni doped Sr_2CuO_3 containing Cu/NiO_4 square planar units. Our polarization-dependent X-ray absorption spectroscopy experiments reveal extremely large orbital polarization ($\sim$63%) for Ni^{2+}, which is the highest value ever reported to the best of our knowledge. Cluster calculations and *ab initio* calculations find that the giant orbital polarization arises due to the low spin S=0 configuration with two holes in Ni $3d_{x^2-y^2}$ orbital, contrary to the expected high spin S=1 state from Hund's first rule.

Transition metal oxides (TMOs) exhibit a variety of tunable electronic, magnetic, and topological phases due to the strong intercoupling among charge, spin, lattice, and orbital degrees of freedom[1–3]. In particular, large orbital polarization plays a decisive role in giving rise to several interesting phenomena in various TMOs, including charge density wave instabilities and metal-insulator transitions in titanates, vanadates, and nickelates[4–7]; emergent magnetic phases in titanates, and manganites[8–10]; and high T_c superconductivity in cuprates[2,11,12]. Designing new materials to achieve large orbital polarization has become a recurring theme in the contemporary condensed matter physics[13–19]. After the theoretical prediction of achieving cuprate like Fermi surface in a three-dimensional compound $LaNiO_3$ through orbital engineering[20–22], various types of artificial structures of $RENiO_3$ (RE: rare-earth elements) family have been extensively investigated[7,13–15]. However, the observed orbital polarization in an octahedral symmetry is low ($\leq$ 25%) and superconductivity remains elusive there. The recent finding of superconductivity in Sr doped $NdNiO_2$ having Ni in square planar coordinate is therefore a monumental development[23], and strongly implies that the local structure (O_h vs. D_{4h} in Fig. 1(a)) and the resultant spin and orbital structures of Ni ions play the central role.

This discovery has led to a large number of works within a short span of time to understand the origin and nature of the superconducting phase[24–38]. While the parent members of the superconducting nickelate and cuprate family are isoelectronic (d^9), several key differences have been noted: unlike the antiferromagnetic insulating phase of the cuprate, $NdNiO_2$ is weakly conducting and nonmagnetic[23]; and the superconducting T_c is much smaller compared to the analogous hole-doped $CaCuO_2$[25,26,39]. There is also an ongoing strong debate about the location of doped holes and the nature of the Ni spin state: d^8 and S=1 vs. d^8 and S= 0 vs. Zhang-Rice singlet $d^9\underline{L}$ ($\underline{L}$ denotes a hole in O $2p$ state)[31,33–37,40]. However, the actual scenario is unknown due to very limited amount of experimental work done in this direction. This prompts us to probe other compounds containing both Cu and Ni in four fold coordinated environment of oxygen.

Here, we focus on Sr_2CuO_3 (SCO), where square planar CuO_4 polyhedral units form linear chains along the b axis (Fig. 1(b))[41]. This quasi one-dimensional system undergoes antiferromagnetic ordering around 5 K[42], and exhibits several intriguing phenomena, including spin-charge separation[43], spin-orbital separation[44], spin Seebeck effect[45], and superconductivity by incorporating excess oxygen[46]. Electronic structure investigations have revealed that Cu in SCO has an extremely small value of the charge transfer energy (Δ)[47–50]. It implies that the ground state of Cu^{2+} in SCO consists of a linear combination of d^9 and dominant $d^{10}\underline{L}$ configurations-contrary to the pure d^9 state expected from an ionic picture[51]. Interestingly, one can replace a small fraction of Cu of SCO with Ni without modifying the structure[52], providing us a unique platform to compare the electronic structure of Cu and Ni within a square planar environment.

In this paper, we investigate the electronic and magnetic structure of Sr_2CuO_3 (SCO) and $Sr_2Cu_{0.9}Ni_{0.1}O_3$ (SCNO) single crystals by magnetic measurement, synchrotron based X-ray linear dichroism (XLD) measurements, density functional theory (DFT) and cluster calculations. We report extremely large orbital polarization of Ni in $Sr_2Cu_{0.9}Ni_{0.1}O_3$ single crystal, which arises due to the low spin S=0 configuration with completely unoccupied $3d_{x^2-y^2}$ orbitals of Ni^{2+}. Ni doping of SCO also enhances the contribution of d^9 configuration in the ground state of Cu^{2+}.

Single crystals of SCO and SCNO were grown using the traveling solvent floating zone technique[55]. All the experiments reported here are carried out on as grown crystals. The magnetic susceptibility was measured using a Physical Property Measurement System, Quantum Design, USA. X-ray absorption spectra (XAS) with vertically (V) and horizontally (H) polarized X-ray were recorded at room temperature in 4-ID-C beamline of Advanced Photon Source, USA.

We first discuss the results of polarization dependent XAS experiment on Cu $L_{3,2}$ edges[11,12,56,57]. XAS (I_{ab}) of SCO (Fig. 1(c)) recorded with in-plane (H) polarized light consists of sharp peaks around 930.5 eV and 950.5 eV, which are associated with the transition from the spin-orbit split Cu $2p_{3/2}$ and Cu $2p_{1/2}$ core levels, respectively, and the final state configuration is $\underline{2p}3d^{10}$ ($\underline{2p}$ denotes a core hole in Cu $2p$ states). The much lower intensity of these peaks in XAS (I_c) with the out-of-plane (V) polarization signifies that the upper Hubbard

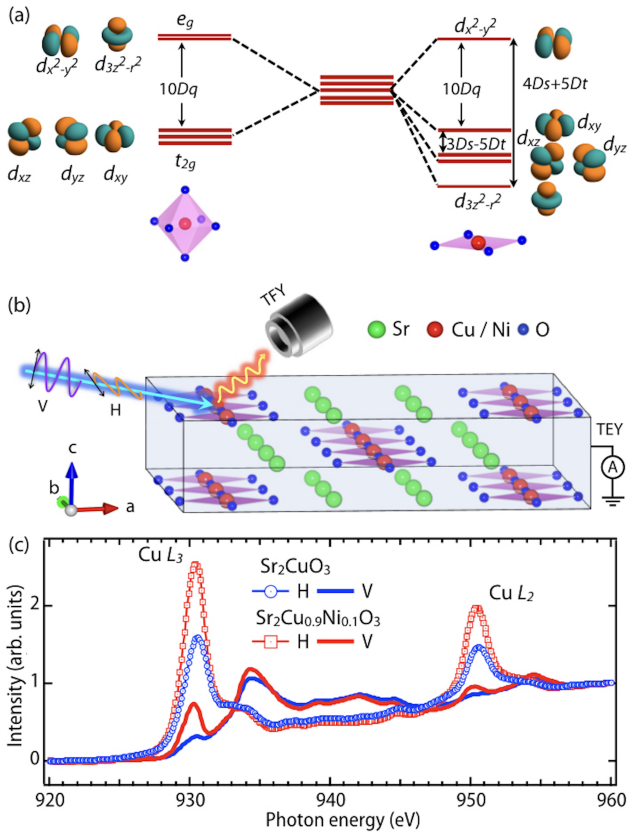


FIG. 1. (a) Energy level splitting of transition metal d orbitals due to point-charge (Coulomb) contributions under octahedral (O_h) and square planar (D_{4h}) environment[53]. The ordering of these levels can be modified in solids due to the hybridization between transition metal d and oxygen p states[54]. (b) Crystal structure of $Sr_2(Cu,Ni)O_3$ and experimental arrangement for XAS experiment with out-of-plane (V) and in-plane (H) polarized X-ray. TFY and TEY denote total fluorescence yield and total electron yield, respectively. (c) Cu $L_{3,2}$-edges XAS recorded in bulk sensitive TFY mode with V, and H X-ray.

band (UHB) is predominately contributed by Cu $d_{x^2-y^2}$ orbitals. The features around 934 eV and 954.5 eV, which are much stronger for the out-of-plane polarization, are related to the transitions into Cu $3d_{3z^2-r^2}$ derived states, which become partially unoccupied due to the hybridization with Cu $4s$ states[57]. Upon Ni doping, the intensity of the white line increases significantly for both polarizations though the line shape remains unchanged (Fig. 1(c)).

Results of polarization dependent XAS experiments at Ni $L_{3,2}$ edges of SCNO at 300 K have been shown in Fig. 2(a). The two intense peaks around 853 eV & 870 eV in the spectrum, recorded with the in-plane polarization (I_{ab}) , correspond to the transitions from Ni $2p_{3/2}$ and Ni $2p_{1/2}$ core levels respectively. I_c, recorded with the out-plane polarization shows significantly low intensity indicating that the holes predominantly occupy the $d_{x^2-y^2}$ bands. The peaks around 856 eV and 874 eV, show higher intensity in I_c than I_{ab}. These features are related to the hybridization of Ni

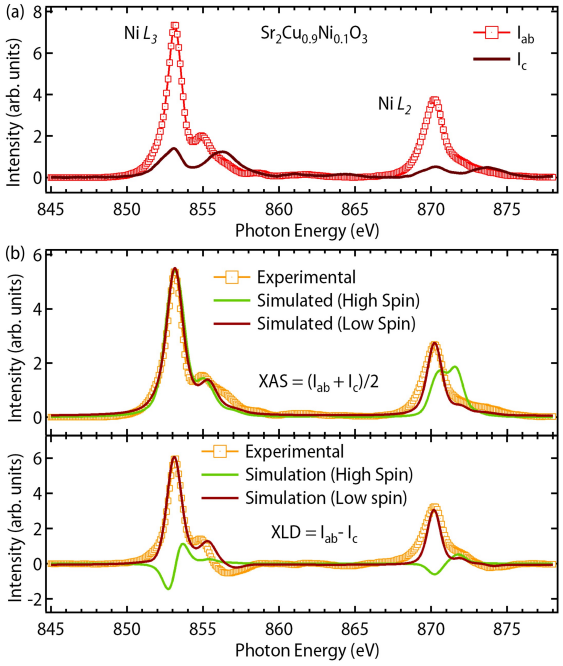


FIG. 2. (a) Ni L_3 and L_2 XAS (TFY mode) for $Sr_2Cu_{0.9}Ni_{0.1}O_3$, recorded with V and H polarization. These spectra have been plotted after background subtraction (Supplemental Material (SM)[58]) (b) Top (bottom) panel: Experimentally observed isotropic XAS (XLD) and simulated XAS (XLD) spectra. The simulation is done for Ni^{2+} with S=1 and S=0 configuration.

TABLE I. Comparison of hole ratio for Ni $3d_{x^2-y^2}$ and Ni $3d_{3z^2-r^2}$ orbitals and % of holes in Ni $3d_{x^2-y^2}$ for $Sr_2Cu_{0.9}Ni_{0.1}O_3$ with literature.

System	X . .	% of holes in Ni $d_{x^2-y^2}$	Reference
$SrCuO_2/LaNiO_3$	0.7	59%	16
$LaTiO_3/LaNiO_3/LaAlO_3$	0.55	65%	17
$La_4Ni_3O_8$	0.4-0.5	67-71%	18
$Sr_2Cu_{0.9}Ni_{0.1}O_3$	0.23	81%	present work

$3d_{3z^2-r^2}$ and Ni $4s$ states. Since the experimental realization of large orbital polarization (OP) in Ni based oxides, with important implications for superconductivity, has been a topic of paramount interest[15–18], we have further evaluated OP of Ni in the present case. According to the sum rule of linear polarization[15–19,64], the ratio of holes in $d_{3z^2-r^2}$ and $d_{x^2-y^2}$ is defined as $X = \frac{h_{3z^2-r^2}}{h_{x^2-y^2}} = \frac{3I'_c}{4I'_{ab}-I'_c}$ with $I'_{ab,c}=\int I_{ab,c}(E)dE$. By this definition, X=1 corresponds to equal hole population in $d_{3z^2-r^2}$ and $d_{x^2-y^2}$ orbitals and X= 0 signifies 100% $d_{x^2-y^2}$ character of holes. We have obtained $X \approx 0.23$ (also see SM[58]) in the present case. This implies 81% of the holes occupy Ni $3d_{x^2-y^2}$ orbital, which is the highest among the existing literature of Ni based complex oxides (see Table I).

The orbital polarization (P) is defined in the literature[15] in terms of the electronic occupation as $P = \frac{n_{3z^2-r^2}-n_{x^2-y^2}}{n_{3z^2-r^2}+n_{x^2-y^2}} =$

$\left(\frac{4}{n'}-1\right)\frac{(1-X)}{(1+X)}$ where $n_{x^2-y^2}$= 2 - $h_{x^2-y^2}$ and $n_{3z^2-r^2}$=2 - $h_{3z^2-r^2}$ are the number of electrons in $d_{x^2-y^2}$ and $d_{3z^2-r^2}$ orbitals, respectively. It is important to note that the value of n' (=$n_{x^2-y^2}$ + $n_{3z^2-r^2}$) can not be determined unambiguously for many compounds due to the presence of charge transfer from O $2p$ to Ni $3d$ orbitals[15,65]. In the present case, $n' \sim 2$ as the ground state wavefunction is dominantly contributed by the d^8 configuration. We have obtained $P \approx 63\%$ for the SCNO, which is also larger compared to all existing literatures on Ni based complex oxides (Table I)[7,15–18,66].

In order to understand the origin of this unprecedentedly large orbital polarization, we have calculated XAS [(I_{ab} + I_c)/2] and XLD [I_{ab}-I_c] of Ni $L_{3,2}$ edges considering a NiO_4 cluster with D_{4h} symmetry and Ni^{2+} ionic configuration using CTM4XAS[67] and Quanty [68] programs that incorporate ligand field multiplet theory. We have simulated for the high spin S = 1 configuration [69,70] (all parameters, used for the simulations have been listed in Ref. 71). Clearly, neither the simulated XAS nor the XLD (Fig. 2(b)) matches with the corresponding experimental spectrum. In particular, the experimentally observed L_2-edge XAS shows only one peak around 870 eV, whereas the simulated spectra shows two peaks. The shape of the simulated XLD is completely different compared to the experimental data. We have also simulated XAS and XLD for the low spin configuration (S = 0) by adjusting crystal field parameters[71], which ensures the following expected crystal field splitting $d_{3z^2-r^2} < d_{xz/yz} < d_{xy} < d_{x^2-y^2}$ for a square planar environment[53]. The excellent matching (Fig. 2(c)) between the experimentally observed and simulated spectra with low spin configuration establishes Ni^{2+} is in S=0 state in the square planar environment.

Simulated spectra with $U > \Delta$ also do not match with experimental observation (see SM for XAS and XLD simulations for different value of Δ considering U=7 eV[58]). We estimate $\Delta \sim$ 7-9 eV in present case, implying electronically NiO_4 belongs near the boundary between Mott Hubbard insulating region and charge transfer insulating region of Zaanen-Sawatzky-Allen phase diagram[24,40,47]. Due to the large Δ, Ni d is less hybridized with O p, compared to the Cu d-O p hybridization. Thus, the replacement of a fraction of Cu by Ni pushes holes from O p towards Cu d around the dopant Ni. This enhances the relative contribution of d^9 configuration, resulting in the observed strong increase in the white line intensity in Cu XAS upon Ni doping (Fig. 1(c)).

The increase of the d^9 component of Cu due to the presence of nonmagnetic Ni^{2+} is also evident in bulk magnetic measurements. The low-temperature magnetic susceptibility (χ) plots of pristine, 1%, and 10% Ni doped SCO samples are shown in Fig. 3. As expected, χ of SCO is very small due to the antiferromagnetic coupling between the neighboring Cu spins. Upon Ni doping, the -O-Cu-O-Cu-O- chain breaks into finite length segments due to an effective spin 0 on the Ni ion. The number of segments thus produced being p+1$\sim p$ for large p, where p is the concentration of Ni. Assuming a statistically random distribution of Ni ions over the chain length, it is reasonable to consider that one-half of the chain segments will have an odd number of Cu spins, and even for the remaining. Since Cu-spins are antiferromagnetically paired, the net

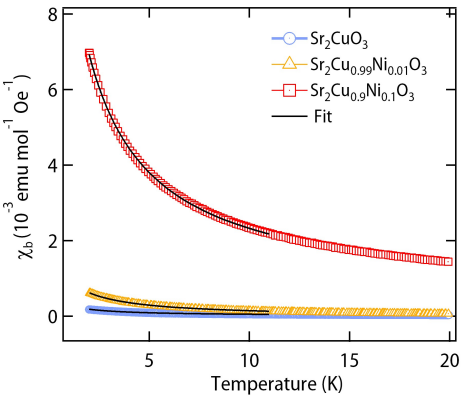


FIG. 3. Temperature dependence of magnetic susceptibility (χ) and fitting by Curie-Weiss (CW) law. For details, see Ref. 52, 72–75. The data for 1% Ni doped SCO sample has been adapted from Ref. 52.

moment on the even-length segments tends to 0 at sufficiently low-temperatures[76]. In contrast, the odd-length segments remain with an uncompensated Cu spin, which results in an enhancement in the magnetic response of Ni doped samples, as seen in Fig. 3. A very weak Curie-tail in the pristine sample can be attributed to the presence of intrinsic defects. We fitted the low-temperature susceptibility of our samples using the Curie-Weiss (CW) law: χ=χ_0+ $C/(T-\theta_{CW})$ where χ_0 is the temperature independent contribution arising due to Van Vleck paramagnetism and core diamagnetism, C is the Curie-constant, and θ_{CW} is the Weiss temperature. The best fit parameters for the three samples are tabulated in SM[58]. From C, the $\mu_{\rm eff}$ (=$\sqrt{8C}$) for the two Ni doped samples (p = 0.01 and 0.1) turned out to be $\sim$ 0.12 μ_B and $\sim$ 0.38 μ_B per formula unit, respectively. The average effective moment on the odd-length segments (=$\sqrt{8C/(0.5p)}$) turns out to be 1.74 μ_B and 1.70 μ_B, respectively for the two samples. These values are close to an effective moment of $\sim$ 1.73 μ_B expected for a S = 1/2 (d^9) system, confirming our conclusion of Cu XAS measurement.

To obtain a microscopic understanding of our experimental observations, we have carried out first-principles density functional theory (DFT) calculations for Sr_2CuO_3 and $Sr_2Cu_{0.875}Ni_{0.125}O_3$ [details are in SM[58]]. The calculated orbital projected density of states (DOS) are shown in Fig. 4. In contrast with the transition metal oxides with positive Δ, the bonding states of SCO are primarily contributed by Cu d orbitals due to negative Δ[54]. The Cu d_{xy}, d_{xz}, d_{yz} and $d_{3z^2-r^2}$ bonding states are spread around 6 eV below the Fermi level (Fig. 4(b)). The valence band and conduction band edge of undoped SCO comes predominantly from O p states (inset of Fig. 4(a)), as expected for a covalent insulator[50]. The $d_{x^2-y^2}$ antibonding states are partially unoccupied, in line with our XAS results. We find that the magnetic moment on Cu is close to 0.19 μ_B. The slight overestimation of this moment, compared to the experimentally observed moment ($\sim 0.06\mu_B$)[42] is likely to be related to the presence of the quantum fluctuation effects in SCO, which are not accounted for in a mean field

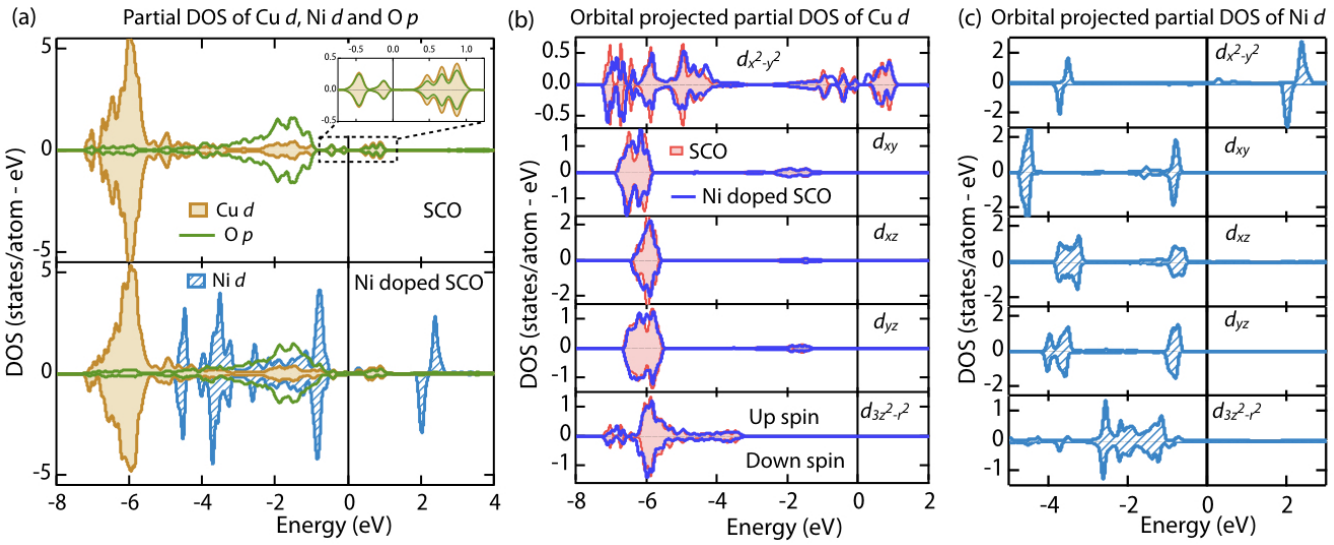


FIG. 4. Orbital projected partial density of states: (a) comparison of DOS of Cu-d, O-p states of undoped SCO (upper panel) with DOS of Cu-d, O-p and Ni-d states of Ni doped SCO (lower panel), (b) comparison of different Cu d-states of doped (line) and undoped (line + shaded) SCO, (c) different d-orbital projected DOS of Ni in doped SCO. The vertical line at zero energy indicates the Fermi level.

approach like DFT. The much smaller moment, compared to the expected moment of 1.73μ_B for a pure d^9 (S=1/2) configuration, again signifies that the ground state of Cu^{2+} in SCO is predominantly $d^{10}\underline{L}$ configuration with small admixture with d^9.

Our DFT calculations of 12.5% Ni doped SCO obtain Cu magnetic moments ranging from 0.13 to 0.24 μ_B and a net moment of $\sim$ 0.13 μ_B per formulae unit. This also supports our observation about the increase of white line intensity of Cu XAS (Fig. 1(c)) and magnetic measurement i.e. the enhancement of d^9 configuration of Cu upon Ni doping. For Ni doped SCO, the contribution arising from different Ni d orbitals is shown in Fig. 4(c) (also see lower panel of Fig. 4(a)). The antibonding states of Ni $d_{x^2-y^2}$ orbital are completely unoccupied, while all other Ni 3d states are completely filled. This low spin S=0 configuration of Ni with holes in the $d_{x^2-y^2}$ orbital is in excellent agreement with our experimental observations.

To summarize, our element sensitive X-ray absorption spectroscopy experiments with linearly polarized light on $Sr_2Cu_{0.9}Ni_{0.1}O_3$ have found that 81% holes of Ni^{2+} sites occupy the $d_{x^2-y^2}$ orbital, which is the highest among all Ni containing oxides reported so far. Ni doping in Sr_2CuO_3 also results in hole transfer from O p to Cu d orbitals. Cluster calculations have revealed that the observed giant orbital polarization arises due to the low spin (S=0) configuration of Ni^{2+}. This nonmagnetic state of Ni^{2+} has been further corroborated by *ab initio* theory.

Finally, we also note that our investigated system has several parallels with the recently discovered superconducting nickelates. Ionically, Sr doping in $NdNi^{+1}O_2$ would result equivalent amount Ni with +2 oxidation state. Our system comprises of NiO_4 units forming one dimensional chains, while the superconducting nickelates have a two dimensional NiO_2 plane. It is expected that the increase in the dimensionality of the system would further enhance Δ[77], and therefore our conclusions about the electronic structure of Ni^{2+} should also hold for nickelate superconductors.

Note added: During the review of this paper, a preprint appeared about XAS and RIXS (resonant inelastic X-ray scattering) study of $Nd_{1-x}Sr_xNiO_2$[78], which also reports that the doped holes are in Ni $3d_{x^2-y^2}$ orbital with a d^8 S=0 state.

Acknowledgement: SM thanks Tanmoy Das and H. R. Krishnamurthy for discussions. SM acknowledges financial support from a SERB Early Career Research Award (ECR/2018/001512) and MHRD STARS 156/2019 project for research funding. SM also thanks the Department of Science and Technology, India (No. SR/NM/Z-07/2015) for the financial support to conduct the synchrotron experiment at the Advanced Photon Source and Jawaharlal Nehru Centre for Advanced Scientific Research (JNCASR) for managing the project. This research used resources of the Advanced Photon Source, a U.S. Department of Energy Office of Science User Facility operated by Argonne National Laboratory under Contract No. DE-AC02-06CH11357. AN acknowledges support from the start-up grant (SG/MHRD-19-0001) of the Indian Institute of Science.

* Contributed equally
† Corresponding author. Email: smiddey@iisc.ac.in

[1] M. Imada, A. Fujimori, and Y. Tokura, Rev. Mod. Phys. **70**, 1039 (1998).

[2] B. Keimer, S. A. Kivelson, M. R. Norman, S. Uchida, and J. Zaanen, Nature **518**, 179 (2015).
[3] Y. Tokura, M. Kawasaki, and N. Nagaosa, Nature Physics **13**, 1056 (2017).
[4] C. F. Chang, T. C. Koethe, Z. Hu, J. Weinen, S. Agrestini, L. Zhao, J. Gegner, H. Ott, G. Panaccione, H. Wu, M. W. Haverkort, H. Roth, A. C. Komarek, F. Offi, G. Monaco, Y.-F. Liao, K.-D. Tsuei, H.-J. Lin, C. T. Chen, A. Tanaka, and L. H. Tjeng, Phys. Rev. X **8**, 021004 (2018).
[5] M. W. Haverkort, Z. Hu, A. Tanaka, W. Reichelt, S. V. Streltsov, M. A. Korotin, V. I. Anisimov, H. H. Hsieh, H.-J. Lin, C. T. Chen, D. I. Khomskii, and L. H. Tjeng, Phys. Rev. Lett. **95**, 196404 (2005).
[6] N. B. Aetukuri, A. X. Gray, M. Drouard, M. Cossale, L. Gao, A. H. Reid, R. Kukreja, H. Ohldag, C. A. Jenkins, E. Arenholz, K. P. Roche, H. A. Drr, M. G. Samant, and S. S. P. Parkin, Nature Physics **9**, 661 (2013).
[7] S. Middey, J. Chakhalian, P. Mahadevan, J. W. Freeland, A. J. Millis, and D. D. Sarma, Annual Review of Materials Research **46**, 305 (2016).
[8] J. Garcia-Barriocanal, J. Cezar, F. Bruno, P. Thakur, N. Brookes, C. Utfeld, A. Rivera-Calzada, S. Giblin, J. Taylor, J. Duffy, S. Dugdale, T. Nakamura, K. Kodama, C. Leon, S. Okamoto, and J. Santamaria, Nature Communications **1** (2010), 10.1038/ncomms1080.
[9] P. Yu, J.-S. Lee, S. Okamoto, M. D. Rossell, M. Huijben, C.-H. Yang, Q. He, J. X. Zhang, S. Y. Yang, M. J. Lee, Q. M. Ramasse, R. Erni, Y.-H. Chu, D. A. Arena, C.-C. Kao, L. W. Martin, and R. Ramesh, Phys. Rev. Lett. **105**, 027201 (2010).
[10] M. Salluzzo, S. Gariglio, D. Stornaiuolo, V. Sessi, S. Rusponi, C. Piamonteze, G. M. De Luca, M. Minola, D. Marré, A. Gadaleta, H. Brune, F. Nolting, N. B. Brookes, and G. Ghiringhelli, Phys. Rev. Lett. **111**, 087204 (2013).
[11] N. Nücker, E. Pellegrin, P. Schweiss, J. Fink, S. L. Molodtsov, C. T. Simmons, G. Kaindl, W. Frentrup, A. Erb, and G. Müller-Vogt, Phys. Rev. B **51**, 8529 (1995).
[12] J. Chakhalian, J. W. Freeland, H.-U. Habermeier, G. Cristiani, G. Khaliullin, M. van Veenendaal, and B. Keimer, Science **318**, 1114 (2007), http://www.sciencemag.org/content/318/5853/1114.full.pdf.
[13] J. W. Freeland, J. Liu, M. Kareev, B. Gray, J. W. Kim, P. J. Ryan, R. Pentcheva, and J. Chakhalian, Europhysics Letters **96**, 57004 (2011).
[14] E. Benckiser, M. W. Haverkort, S. Brck, E. Goering, S. Macke, A. Frañó, X. Yang, O. K. Andersen, G. Cristiani, H.-U. Habermeier, A. V. Boris, I. Zegkinoglou, P. Wochner, H.-J. Kim, V. Hinkov, and B. Keimer, Nature Materials **10**, 189 (2011).
[15] M. Wu, E. Benckiser, M. W. Haverkort, A. Frano, Y. Lu, U. Nwankwo, S. Brück, P. Audehm, E. Goering, S. Macke, V. Hinkov, P. Wochner, G. Christiani, S. Heinze, G. Logvenov, H.-U. Habermeier, and B. Keimer, Phys. Rev. B **88**, 125124 (2013).
[16] Z. Liao, E. Skoropata, J. W. Freeland, E.-J. Guo, R. Desautels, X. Gao, C. Sohn, A. Rastogi, T. Z. Ward, T. Zou, T. Charlton, M. R. Fitzsimmons, and H. N. Lee, Nature Communications **10** (2019), 10.1038/s41467-019-08472-y.
[17] A. S. Disa, D. P. Kumah, A. Malashevich, H. Chen, D. A. Arena, E. D. Specht, S. Ismail-Beigi, F. J. Walker, and C. H. Ahn, Phys. Rev. Lett. **114**, 026801 (2015).
[18] J. Zhang, A. S. Botana, J. W. Freeland, D. Phelan, H. Zheng, V. Pardo, M. R. Norman, and J. F. Mitchell, Nature Physics **13**, 864 (2017).
[19] S. Lee, A. T. Lee, A. B. Georgescu, G. Fabbris, M.-G. Han, Y. Zhu, J. W. Freeland, A. S. Disa, Y. Jia, M. P. M. Dean, F. J. Walker, S. Ismail-Beigi, and C. H. Ahn, Phys. Rev. Lett. **123**, 117201 (2019).
[20] V. I. Anisimov, D. Bukhvalov, and T. M. Rice, Phys. Rev. B **59**, 7901 (1999).
[21] J. c. v. Chaloupka and G. Khaliullin, Phys. Rev. Lett. **100**, 016404 (2008).
[22] P. Hansmann, X. Yang, A. Toschi, G. Khaliullin, O. K. Andersen, and K. Held, Phys. Rev. Lett. **103**, 016401 (2009).
[23] D. Li, K. Lee, B. Y. Wang, M. Osada, S. Crossley, H. R. Lee, Y. Cui, Y. Hikita, and H. Y. Hwang, Nature **572**, 624 (2019).
[24] M. Hepting, D. Li, C. Jia, H. Lu, E. Paris, Y. Tseng, X. Feng, M. Osada, E. Been, Y. Hikita, *et al.*, Nature materials **19**, 381 (2020).
[25] D. Li, B. Y. Wang, K. Lee, S. P. Harvey, M. Osada, B. H. Goodge, L. F. Kourkoutis, and H. Y. Hwang, Phys. Rev. Lett. **125**, 027001 (2020).
[26] S. Zeng, C. S. Tang, X. Yin, C. Li, Z. Huang, J. Hu, W. Liu, G. J. Omar, H. Jani, Z. S. Lim, *et al.*, arXiv preprint arXiv:2004.11281 (2020).
[27] A. S. Botana and M. R. Norman, Phys. Rev. X **10**, 011024 (2020).
[28] F. Lechermann, Phys. Rev. B **101**, 081110 (2020).
[29] P. Jiang, L. Si, Z. Liao, and Z. Zhong, Phys. Rev. B **100**, 201106 (2019).
[30] J. Karp, A. S. Botana, M. R. Norman, H. Park, M. Zingl, and A. Millis, arXiv preprint arXiv:2001.06441 (2020).
[31] L.-H. Hu and C. Wu, Phys. Rev. Research **1**, 032046 (2019).
[32] P. Adhikary, S. Bandyopadhyay, T. Das, I. Dasgupta, and T. Saha-Dasgupta, arXiv preprint arXiv:2005.01243 (2020).
[33] M. Jiang, M. Berciu, and G. A. Sawatzky, Phys. Rev. Lett. **124**, 207004 (2020).
[34] Y.-H. Zhang and A. Vishwanath, Phys. Rev. Research **2**, 023112 (2020).
[35] H. Zhang, L. Jin, S. Wang, B. Xi, X. Shi, F. Ye, and J.-W. Mei, Phys. Rev. Research **2**, 013214 (2020).
[36] Z.-J. Lang, R. Jiang, and W. Ku, arXiv preprint arXiv:2005.00022 (2020).
[37] J. Karp, A. S. Botana, M. R. Norman, H. Park, M. Zingl, and A. Millis, arXiv preprint arXiv:2001.06441 (2020).
[38] J. Krishna, H. LaBollita, A. O. Fumega, V. Pardo, and A. S. Botana, arXiv preprint arXiv:2008.02237 (2020).
[39] M. Azuma, Z. Hiroi, M. Takano, Y. Bando, and Y. Takeda, Nature **356**, 775 (1992).
[40] B. H. Goodge, D. Li, M. Osada, B. Y. Wang, K. Lee, G. A. Sawatzky, H. Y. Hwang, and L. F. Kourkoutis, arXiv preprint arXiv:2005.02847 (2020).
[41] N. Motoyama, H. Eisaki, and S. Uchida, Phys. Rev. Lett. **76**, 3212 (1996).
[42] K. M. Kojima, Y. Fudamoto, M. Larkin, G. M. Luke, J. Merrin, B. Nachumi, Y. J. Uemura, N. Motoyama, H. Eisaki, S. Uchida, K. Yamada, Y. Endoh, S. Hosoya, B. J. Sternlieb, and G. Shirane, Phys. Rev. Lett. **78**, 1787 (1997).
[43] R. Neudert, M. Knupfer, M. S. Golden, J. Fink, W. Stephan, K. Penc, N. Motoyama, H. Eisaki, and S. Uchida, Phys. Rev. Lett. **81**, 657 (1998).
[44] J. Schlappa, K. Wohlfeld, K. Zhou, M. Mourigal, M. Haverkort, V. Strocov, L. Hozoi, C. Monney, S. Nishimoto, S. Singh, *et al.*, Nature **485**, 82 (2012).
[45] D. Hirobe, M. Sato, T. Kawamata, Y. Shiomi, K.-i. Uchida, R. Iguchi, Y. Koike, S. Maekawa, and E. Saitoh, Nature Physics **13**, 30 (2017).
[46] .-Z. Hiroi, M. Takano, M. Azuma, and Y. Takeda, Nature **364**, 315 (1993).
[47] J. Zaanen, G. A. Sawatzky, and J. W. Allen, Phys. Rev. Lett. **55**, 418 (1985).
[48] S. Nimkar, D. D. Sarma, H. R. Krishnamurthy, and S. Ramasesha,

Phys. Rev. B **48**, 7355 (1993).
[49] K. Maiti, D. D. Sarma, T. Mizokawa, and A. Fujimori, Europhysics Letters (EPL) **37**, 359 (1997).
[50] K. Maiti, D. D. Sarma, T. Mizokawa, and A. Fujimori, Phys. Rev. B **57**, 1572 (1998).
[51] A. C. Walters, T. G. Perring, J.-S. Caux, A. T. Savici, G. D. Gu, C.-C. Lee, W. Ku, and I. A. Zaliznyak, Nature Physics **5**, 867 (2009).
[52] K. Karmakar and S. Singh, Phys. Rev. B **91**, 224401 (2015).
[53] M. M. Sala, V. Bisogni, C. Aruta, G. Balestrino, H. Berger, N. B. Brookes, G. M. de Luca, D. D. Castro, M. Grioni, M. Guarise, P. G. Medaglia, F. M. Granozio, M. Minola, P. Perna, M. Radovic, M. Salluzzo, T. Schmitt, K. J. Zhou, L. Braicovich, and G. Ghiringhelli, New Journal of Physics **13**, 043026 (2011).
[54] A. V. Ushakov, S. V. Streltsov, and D. I. Khomskii, Journal of Physics: Condensed Matter **23**, 445601 (2011).
[55] K. Karmakar, R. Bag, and S. Singh, Crystal Growth & Design **15**, 4843 (2015).
[56] M. Knupfer, R. Neudert, M. Kielwein, S. Haffner, M. S. Golden, J. Fink, C. Kim, Z.-X. Shen, M. Merz, N. Nücker, S. Schuppler, N. Motoyama, H. Eisaki, S. Uchida, Z. Hu, M. Domke, and G. Kaindl, Phys. Rev. B **55**, R7291 (1997).
[57] R. Neudert, S.-L. Drechsler, J. Málek, H. Rosner, M. Kielwein, Z. Hu, M. Knupfer, M. S. Golden, J. Fink, N. Nücker, M. Merz, S. Schuppler, N. Motoyama, H. Eisaki, S. Uchida, M. Domke, and G. Kaindl, Phys. Rev. B **62**, 10752 (2000).
[58] See Supplemental Material for multiplet cluster calculations, extraction of orbital polarization, analysis of magnetic susceptibilities and details of DFT calculations, which includes Ref. 59–63.
[59] J. H. Van Vleck, *The theory of electric and magnetic susceptibilities* (Clarendon Press, 1932).
[60] P. Giannozzi, S. Baroni, N. Bonini, M. Calandra, R. Car, C. Cavazzoni, D. Ceresoli, G. L. Chiarotti, M. Cococcioni, I. Dabo, A. D. Corso, S. de Gironcoli, S. Fabris, G. Fratesi, R. Gebauer, U. Gerstmann, C. Gougoussis, A. Kokalj, M. Lazzeri, L. Martin-Samos, N. Marzari, F. Mauri, R. Mazzarello, S. Paolini, A. Pasquarello, L. Paulatto, C. Sbraccia, S. Scandolo, G. Sclauzero, A. P. Seitsonen, A. Smogunov, P. Umari, and R. M. Wentzcovitch, Journal of Physics: Condensed Matter **21**, 395502 (2009).
[61] J. P. Perdew, K. Burke, and M. Ernzerhof, Phys. Rev. Lett. **77**, 3865 (1996).
[62] D. Vanderbilt, Physical Review B **41**, 7892 (1990).
[63] M. Cococcioni and S. de Gironcoli, Phys. Rev. B **71**, 035105 (2005).
[64] G. Van der Laan, Journal of the Physical Society of Japan **63**, 2393 (1994).
[65] O. E. Peil, M. Ferrero, and A. Georges, Phys. Rev. B **90**, 045128 (2014).
[66] S. Middey, D. Meyers, D. Doennig, M. Kareev, X. Liu, Y. Cao, Z. Yang, J. Shi, L. Gu, P. J. Ryan, R. Pentcheva, J. W. Freeland, and J. Chakhalian, Phys. Rev. Lett. **116**, 056801 (2016).
[67] E. Stavitski and F. M. De Groot, Micron **41**, 687 (2010).
[68] M. Retegan, "Crispy: v0.7.3," (2019).
[69] Y. Utz, F. Hammerath, R. Kraus, T. Ritschel, J. Geck, L. Hozoi, J. van den Brink, A. Mohan, C. Hess, K. Karmakar, S. Singh, D. Bounoua, R. Saint-Martin, L. Pinsard-Gaudart, A. Revcolevschi, B. Bchner, and H.-J. Grafe, Physical Review B **96** (2017), 10.1103/physrevb.96.115135.
[70] G. van der Laan, B. T. Thole, G. A. Sawatzky, and M. Verdaguer, Phys. Rev. B **37**, 6587 (1988).
[71] Δ = 9 eV, U_{dd} = 7 eV, U_{pd} = 9 eV were used in Cluster calculations. The hopping parameters, related to d_{z^2}, $d_{x^2-y^2}$, d_{xy} and d_{xz}/d_{yz} orbitals, were chosen to be 2.0, 2.0, 1.0, 1.0 eV, respectively. For the high spin (S = 1) configuration, the crystal field parameters for D_{4h} symmetry were chosen as Dq = 0.235 eV, Ds = 0.1 eV, Dt = 0.05 eV. Whereas, Dq = 0.235 eV, Ds = 0.52 eV, Dt = 0.3 eV were used for the low spin (S = 0) configuration.
[72] In principle, depending on the temperature range, one should also include not only the chain susceptibility, i.e., the susceptibility of an endless antiferromagnetic chain[73], but also the boundary contribution arising from the staggered moment at the free ends of a chain segment[52,74]. However as shown by Sirker et al., the generalized expression of χ, including all the terms mentioned above, reduces to the CW equation in the low-temperature limit[75]. Hence, we used the data below 10 K and fitted that to CW equation for obtaining the effective moment from which the spin state of Ni can be inferred.
[73] D. C. Johnston, R. K. Kremer, M. Troyer, X. Wang, A. Klümper, S. L. Bud'ko, A. F. Panchula, and P. C. Canfield, Phys. Rev. B **61**, 9558 (2000).
[74] S. Fujimoto and S. Eggert, Phys. Rev. Lett. **92**, 037206 (2004).
[75] J. Sirker, N. Laflorencie, S. Fujimoto, S. Eggert, and I. Affleck, Phys. Rev. Lett. **98**, 137205 (2007).
[76] T. Ami, M. K. Crawford, R. L. Harlow, Z. R. Wang, D. C. Johnston, Q. Huang, and R. W. Erwin, Phys. Rev. B **51**, 5994 (1995).
[77] K. Maiti, P. Mahadevan, and D. D. Sarma, Phys. Rev. B **59**, 12457 (1999).
[78] M. Rossi, H. Lu, A. Nag, D. Li, M. Osada, K. Lee, B. Wang, S. Agrestini, M. Garcia-Fernandez, Y.-D. Chuang, *et al.*, arXiv preprint arXiv:2011.00595 (2020).